Author/s:
Zhang, X;Wang, YP;Peng, S;Rayner, PJ;Ciais, P;Silver, JD;Piao, S;Zhu, Z;Lu, X;Zheng, X

Title:
Dominant regions and drivers of the variability of the global land carbon sink across timescales

Date:
2018-09-01

Citation:
Zhang, X., Wang, Y. P., Peng, S., Rayner, P. J., Ciais, P., Silver, J. D., Piao, S., Zhu, Z., Lu, X. & Zheng, X. (2018). Dominant regions and drivers of the variability of the global land carbon sink across timescales. Global Change Biology, 24 (9), pp.3954-3968. https://doi.org/10.1111/gcb.14275.

DR. SHUSHI PENG (Orcid ID : 0000-0001-5098-726X)
DR. SHILONG PIAO (Orcid ID : 0000-0001-8057-2292)



Article type : Primary Research Articles

Article Type: Primary Research Articles

# Dominant regions and drivers of the variability of the global land carbon sink across timescales

**Xuanze Zhang[1], Ying-Ping Wang[2,3], Shushi Peng[1,*], Peter J. Rayner[4], Philippe Ciais[5], Jeremy D. Silver[4], Shilong Piao[1,6,7], Zaichun Zhu[1], Xingjie Lu[8], Xiaogu Zheng[9]**

[1] Sino-French Institute for Earth System Science, College of Urban and Environmental Sciences, Peking University, Beijing 100871, China

[2] South China Botanical Garden, Chinese Academy of Sciences, Guangzhou 510650, China

[3] CSIRO Oceans and Atmosphere, Private Bag 1, Aspendale, Victoria 3195, Australia

[4] School of Earth Sciences, University of Melbourne, Melbourne, Victoria 3010, Australia

[5] Laboratoire des Sciences du Climat et de l'Environnement, LSCE/IPSL, CEA-CNRS-UVSQ, Université Paris-Saclay, 91191 Gif-sur-Yvette, France

[6] Key Laboratory of Alpine Ecology and Biodiversity, Institute of Tibetan Plateau Research, Chinese Academy of Sciences, Beijing 100085, China

[7] Center for Excellence in Tibetan Plateau Earth Science, Chinese Academy of Sciences, Beijing 100085, China

[8] Department of Botany and Microbiology, University of Oklahoma, Norman, OK 73019, USA

[9] Institute of Atmospheric Physics, Chinese Academy of Sciences, Beijing 100029, China

[*]Correspondence: Shushi Peng, Email: speng@pku.edu.cn.

**Running title**: Variability of land carbon sink

**Keywords:** global carbon cycle, land carbon sink, DGVM, variability, PDO, ENSO

## Abstract

Net biome productivity (NBP) dominates the observed large variation of atmospheric $CO_2$ annual increase over the last five decades. However, the dominant regions controlling inter-annual to multi-decadal variability of global NBP are still controversial (semi-arid regions vs. temperate or tropical forests). By developing a theory for partitioning the variance of NBP into the contributions of net primary production (NPP) and heterotrophic respiration ($R_h$) at different timescales, and using both observation-based atmospheric $CO_2$ inversion product and the outputs of 10 process-based terrestrial ecosystem models forced by 110-year observational climate, we tried to reconcile the controversy by showing that semi-arid lands dominate the variability of global NBP at inter-annual (<10 years) and tropical forests dominate at multi-decadal scales (>30 years). Results further indicate that global NBP variability is dominated by the NPP component at inter-annual timescales, and is progressively controlled by $R_h$ with increasing timescale. Multi-decadal NBP variations of tropical rainforests are modulated by the Pacific Decadal Oscillation (PDO) through its significant influences on both temperature and precipitation. This study calls for long-term observations for the decadal or longer fluctuations in carbon fluxes to gain insights on the future evolution of global NBP, particularly in the tropical forests that dominate the decadal variability of land carbon uptake and are more effective for climate mitigation.

## INTRODUCTION

The growth of atmospheric $CO_2$ concentration has been effectively slowed down by the land carbon sink, which absorbed about 30% of anthropogenic $CO_2$ emissions during the past five decades (Le Quéré *et al.*, 2014, Le Quéré *et al.*, 2009). Without this land carbon sink, our present climate would be 30% or 0.3 K warmer (Shevliakova *et al.*, 2013). The global atmosphere-to-land $CO_2$ uptake, also defined as net biome productivity (NBP), is a small difference between carbon uptake by net primary production (NPP) and the release from heterotrophic respiration ($R_h$) and disturbance emissions including fires (D) (NBP=NPP-$R_h$-D). In the past two decades, besides significant progresses to address the conundrum of "where does anthropogenic carbon go" (Gurney *et al.*, 2002, Jacobson *et al.*, 2007, Pan *et al.*, 2011, Peylin *et al.*, 2013, Schimel, 2007), two new important questions about terrestrial carbon sinks emerged, inter-annual variability and trend (Anderegg *et al.*, 2015, Le Quéré *et al.*, 2014, Le Quéré *et al.*, 2009, Wang *et al.*, 2013). Tropical forests were regarded as the dominant regions driving inter-annual variability of global NBP and therefore atmospheric $CO_2$ growth rate (Cox *et al.*, 2013, Le Quéré *et al.*, 2009, Liu *et al.*, 2017, Wang *et al.*, 2013). But this view was challenged by recent studies (Ahlström *et al.*, 2015, Poulter *et al.*, 2014) that suggested that semi-arid ecosystems (including all savannah and shrub lands in southern hemisphere and between the equator to 45$^{o}$N) dominated the inter-annual variability of global land carbon sink over the last three decades. Increased trend of global land carbon sink were observed during the last three decades (Le Quéré *et al.*, 2014, Le Quéré *et al.*, 2009), hence tropical forests (Pan *et al.*, 2011), northern forests (Forkel *et al.*, 2016, Graven *et al.*, 2013) and semi-arid lands (Ahlström *et al.*, 2015) were also proposed to be the dominant land carbon sinks. Thus which regions dominated the inter-annual or decadal to multi-decadal variability of global land carbon sink, and what their contributions or drivers were over the last three to five decades are being vigorously debated within the science community (Ahlström *et al.*, 2015, Anderegg *et al.*, 2015, Cox *et al.*, 2013, Gurney *et al.*, 2008, Pan *et al.*, 2011, Poulter *et al.*, 2014, Sitch *et al.*, 2015, Wang *et al.*, 2013).

To be able to quantify the regional contributions to global NBP and their variations is critically important for further understanding the mechanisms of land carbon accumulation and the recently proposed spatially diversified strategy for

climate change mitigation (Tubiello, 2012). Because of the large variations of carbon residence time among different terrestrial ecosystems (Bloom *et al.*, 2016), new theory and methods linking variations of NBP and their drivers are needed to reconcile the controversy on regional contributions to variations of global NBP at different timescales. It is possible that the dominant region varies with time scale. For climate mitigation, regions that dominate the global NBP on a long time scale are more effective for carbon sequestration. This time-scale dependence of regional land sink dominance remains unresolved.

Here, we developed a theory based on time domain analysis of the carbon cycle to attribute the variations of NBP to those of NPP, $R_h$ and D across different frequency scales. The theory was applied to the output of 10 dynamic global vegetation models (DGVMs) from the "Trends and drivers of the regional scale sources and sinks of carbon dioxide" (TRENDY) project phase 2 (Piao *et al.*, 2013, Sitch *et al.*, 2015), and the modeled NBP ensemble were compared with the independent estimates from observation-based global land carbon sink and the atmospheric $CO_2$ inversion product, and carbon sources released from bookkeeping-based land use change and fires products over their overlaid periods. To identify the role of plant productivity and soil respiration on land carbon accumulation, the contribution of $R_h$ to NBP variations was further split into two components: one being the NPP-dependent response of $R_h$ as NPP anomalies cause changes of vegetation biomass pools, which are chased to litter and soil carbon pools and impact $R_h$ with a lag effect (e.g. years to decades); And the other component being the direct response of $R_h$ to climate change, as soil temperature and moisture modulate carbon decomposition rates. To further link to climatic drivers of NBP variations across different timescales, we use one of these DGVMs known as CABLE (version 2) (Wang *et al.*, 2010) to quantify the individual effect of each of the seven external variables (temperature, precipitation etc.), nitrogen deposition, and atmospheric $CO_2$. Finally, the linkages between two major global modes of climate variability, the El Niño Southern Oscillation (ENSO) and the Pacific Decadal Oscillation (PDO) and regional/global NBP variations on inter-annual and multi-decadal timescales are investigated.

## MATERIALS AND METHODS

### TRENDY DGVMs historical simulations

We used 110-yers historical simulations of 10 dynamic global vegetation models (DGVMs) including CABLE, CLM4-C, CLIM4-CN, LPJwsl, LPJ-GUESS, OCN, ORCHIDEE, SDGVM, TRIFFID, and VEGAS (see Table S1) from TRENDY V2 project (experiment S2: varying $CO_2$ and climate, experiment S3: varying $CO_2$, climate and land use change). Previous evaluation of the TRENDY ensemble has shown good performance compared to observations (Piao *et al.*, 2013, Sitch *et al.*, 2015). All TRENDY DGVMs were forced by the observational climate CRUNCEP version 5 (New *et al.*, 2002), atmospheric $CO_2$ concentration record (Keeling & Whorf, 2005) and land use change estimates. Datasets can be downloaded from www.globalcarbonproject.org/reccap. CRUNCEP version 5 data is a 6-hourly dataset at a 0.5° × 0.5° resolution of seven climate surface variables (temperature, precipitation, downward shortwave radiation, downward longwave radiation, humidity, pressure and wind speed) over 1901-2010. CRUNCEP is a combination of the CRU TS.3.22 0.5° ×0.5° monthly climatology covering the period 1901–2013 (Mitchell & Jones, 2005), and the 6-hourly NCEP reanalysis 2.5° × 2.5° climatology covering the period 1948 to 2013 (Kalnay *et al.*, 1996). As prior to 1950, CRU is recycling climatology for areas (such as Africa, South America etc.) where the observation network is sparse (Mitchell & Jones, 2005), which may cause land surface modelling uncertainties over these areas. We calculated yearly carbon fluxes (NBP, NPP, $R_h$, Ffire, Fluc) and pools (cVeg, cLitter and cSoil) for each TRENDY model at the 0.5° scale over 1901-2010 for further analysis. The 110-yr averaged residence time for the TRENDY models are found quite different, ranging from 15 years to 31 years, with a mean of 23 years, thus the corresponding averaged turnover rate is 0.043 $yr^{-1}$ (Table S1). To estimate the emissions from land use change, we calculated the difference between the fluxes from the TRENDY S3 and TRENDY S2 ensembles, however we note that only four models (LPJwsl, LPJ-GUESS, OCN, ORCHIDEE) were run in the land use change experiment.

**Observation-based carbon fluxes datasets**

To compare with TRENDY models ensemble NBP, we calculated annual growth rate of difference between the atmospheric $CO_2$ concentration records (Keeling & Whorf, 2005) and fossil-fuel emission statistic estimates (Boden *et al.*, 2016) and the land use and land cover change (LULCC) carbon emissions (Houghton *et al.*, 2012, Houghton & Nassikas, 2017) over 1959-2013. When excluding the carbon sources from human

activities (both fossil and LULCC emissions), the natural atmospheric $CO_2$ growth was only driven by the land and ocean carbon uptake annually.

The estimate of annual global carbon project (GCP) residual land carbon sink over 1959-2013 (Le Quéré *et al.*, 2014, Le Quéré *et al.*, 2009) was also used as a comparison to TRENDY models NBP ensemble. As the GCP residual carbon sink is taken to be the increase in atmospheric $CO_2$ concentration minus all sources (the fossil-fuel and land-use change emissions) and plus known sinks (the ocean carbon sink), it represents an independent estimate of global land carbon sink against the TRENDY models, but the GCP has no estimate at regional scales.

The Copernicus Atmosphere Monitoring Service (CAMS) global atmospheric $CO_2$ inversion (v16r1) is another independent estimate of the land carbon sink with a resolution of 1.9° × 3.75° over 1979-2016, which is an atmosphere-to-land carbon flux product based on the atmospheric $CO_2$ records from global sites, an atmospheric transport model and data assimilation methods (Chevallier *et al.*, 2010). The CAMS inversion has been widely used in carbon cycle and global change fields at global/regional scales (Keenan *et al.*, 2016, Peylin *et al.*, 2013, Poulter *et al.*, 2014). As all the TRENDY models, the GCP and CAMS inversion have accounted for carbon losses from wildfires, thus the satellite-based estimate of the global fire emission database version 4.1s (GFED4) product over 1997-2016 (Giglio *et al.*, 2013) was also compared at global/regional scales.

The TRENDY GPP were compared with observation-based models MODIS GPP (Zhao *et al.*, 2005, Zhao & Running, 2010) and FLUXCOM GPP (Jung *et al.*, 2017) and with the 2001-2010 mean GPP provided by CARDAMOM (Bloom *et al.*, 2016). FLUXCOM GPP is derived using machine learning algorithms on daily carbon flux estimates from 224 flux tower sites with meteorological measurements and satellite and climate data as inputs (Jung *et al.*, 2017). As TRENDY models simulations run until 2010 only in the version we used, and MODIS starts in 2000, we compared GPP over 2000-2010.

**CARDAMOM product for a 10-yr state of ecosystem turnover rates**

The CARDAMOM product is a 10-yr mean state estimate of terrestrial ecosystem carbon fluxes (GPP, NPP, $R_h$, $R_a$, NBP, Ffire etc.), carbon pools (leaf, wood, fine root and labile carbon, litter, soil carbon) and turnover times between carbon pool transfer processes (Bloom *et al.*, 2016). The CARDAMOM data is estimated from an ecosystem-carbon data assimilation framework, utilizing both satellite-based (MODIS LAI, biomass, and wildfire burned areas), and empirically derived global soil carbon data (Harmonized World Soil Database), and station-based FLUXNET data (GPP and residence time etc.) based on the ecosystem carbon balance and allocation box model (Bloom & Williams, 2015). We compared the estimated ecosystem turnover rates derived from the CARDAMOM product with those of the 10-member TRENDY models ensemble over the period of 2001-2010 (Fig. S12).

**A theoretical approach to attribution of NBP variation**

The theory to analyse the contributions of NPP or $R_h$ and D to variations of NBP across all timescales is based on the fact that the terrestrial carbon cycle can be represented by the following equation:

$$\frac{\mathrm{d}C_{\mathrm{eco}}}{\mathrm{d}t} = \mathrm{NBP} = \mathrm{NPP} - \tau C_{\mathrm{eco}} \tag{1}$$

Where the turnover rate of a carbon pool ($\tau$) in units of $yr^{-1}$ is defined by:

$$\tau = \frac{\mathrm{R_h} + \mathrm{D}}{C_{\mathrm{eco}}}. \tag{2}$$

The definition of terrestrial carbon cycle as described in Equation 1 is derived from Taylor and Lloyd (Taylor & Lloyd, 1992). As the year-to-year or decade-to-decade variations of carbon fluxes or other variables in climate system of the Earth are mostly driven by more than one factor on different timescales, fluctuations of these carbon fluxes thus can be seen as the wave superposition over different frequencies. To this end, we assume that time series of NPP and $C_{\mathrm{eco}}$ variations at any time $t$ are compositions from different frequencies:

$$NPP(t) = \sum_k A_k \cos(\omega_k t) \tag{3}$$

$$C_{\mathrm{eco}}(t) = \sum_k a_k \cos(\omega_k t) + b_k \sin(\omega_k t) \tag{4}$$

where $\omega_k = 2\pi \frac{k}{N}$ is the angular frequency, $k$ the wavenumber, $N$ the time period in years, $A_k$ , $a_k$ and $b_k$ the amplitude parameters of NPP and $C_{eco}$ frequencies at each wavenumber. By substituting Equations 3-4 in Equation 1, one can derive analytical solutions for the contribution of NPP and $R_h$ plus D to the variations of NBP (see Supplementary Materials for more details). At any given frequency $\omega$, we have

$$\frac{A_{\mathrm{NBP}}}{A_{\mathrm{NPP}}} = \frac{\omega}{\sqrt{\omega^2 + \tau^2}} \tag{5}$$

$$\frac{A_{\mathrm{R_h+D}}}{A_{\mathrm{NPP}}} = \frac{\tau}{\sqrt{\omega^2 + \tau^2}} \tag{6}$$

where $A_{NBP,}$ $A_{NPP}$, and $A_{Rh+D}$ represent the amplitude of NBP, NPP, and $R_h$ plus D respectively for a given frequency. These equations show that ratio of the amplitude of the variability of NBP to that of $R_h$+D and NPP at a given frequency is determined only by the turnover rate $\tau$ (Fig. S1), predicting that NBP is dominated by NPP at short-term timescales, but not at longer timescales.

From Equations 5-6, at any given frequency $\omega$, the variance of NBP can be further decomposed into the contributions of variances of NPP and $R_h$+D as given by Equation 7,

$$A^2_{\mathrm{NBP}} = A^2_{\mathrm{NPP}} - A^2_{\mathrm{R_h+D}}\,. \tag{7}$$

The relationship between the spectral coefficients and the variance of the corresponding time-series is evident from Equation 7; Integrating the power spectral density (the series of squares of the Fourier coefficients) provides the variance of the series (Thomson & Emery, 2014), that can be decomposed into different timescales. Hence the variances of NPP, NBP and $R_h$+D at any given frequency are equal to $A^2_{\mathrm{NPP}}$, $A^2_{\mathrm{NBP}}$ and $A^2_{\mathrm{R_h+D}}$ respectively. We introduce this spectral analysis for carbon fluxes aiming to identify dominant regions and drivers across different timescales over a given period. In this study, although the global annual mean of wildfires or land use change emissions are ~2 Pg C $yr^{-1}$, we notice that the variance of D from fires and land use change emissions from TRENDY models (Fig. S3b) is almost negligible, being less than 0.2 $(Pg\ C)^2\ yr^{-2}$ across the frequencies from 0.01 $yr^{-1}$ to 0.5 $yr^{-1}$ from 1901 to 2010, compared with the variances of NPP and $R_h$ (Fig. S3). Since $A^2_{\mathrm{D}} << A^2_{\mathrm{R_h}}$ in DGVMs, we assumed $A^2_{\mathrm{R_h+D}} \approx A^2_{\mathrm{R_h}}$ in DGVMs. Note that the uncertainties of this

flux in DGVMs are large (Hantson *et al.*, 2016, van der Werf *et al.*, 2010), especially because that the slow changes in disturbance regimes (fire prevention or amplification by human activities, ecosystem structural changes) are poorly represented in DGVMs (Hantson *et al.*, 2016, Houghton *et al.*, 2012, van der Werf *et al.*, 2010), and emissions from land use change also has large uncertainty, here we also calculated the variance of $A_D^2$ from GFED4 (Giglio *et al.*, 2013) and LULCC (Houghton *et al.*, 2012).

As shown by Equation 6, the variance of $R_h$ at a given frequency depends on the variance of NPP and turnover rate $\tau$. When fixing $\tau$ with varying $A_{NPP}$, the response of $R_h$ to the variance of NPP is defined as NPP-dependent response of $R_h$ through impacting litter and soil carbon pools (hereafter referred to $R_{h1}$); when fixing $A_{NPP}$ with varying $\tau$ due to the impacts of climate change on decomposition rates, the response of $R_h$ to climate change is defined as $R_{h2}$. To separate the contributions of $R_{h1}$ and $R_{h2}$ to the variance of NBP in TRENDY DGVMs ensemble ($NBP_{TRENDY}$), we diagnosed $R_{h1}$ from a reduced-complexity three-pool box model (Box-Model, section 2.2.2) that reproduces the NBP response of each complex DGVM model forced by the NPP and D from the models but with constant $\tau$ excluding the variance of $R_{h2}$ i.e. setting $A_{R_{h2}}^2 = 0$ in the Box-Model. The NBP estimated by the Box-Models with constant $\tau$ hereafter is called $NBP_{TRENDY}^{\tau_{fixed}}$). The term $R_{h2}$ was estimated as the difference of $R_h$ as simulated by the TRENDY models and $R_{h1}$ from the Box-Model.

**Box models for terrestrial carbon cycle**

We developed a three-carbon-pool box model (Box-Model) for diagnosing the behaviour of carbon cycle processes in terrestrial ecosystem models. It allows us to separate contributions of NPP and $R_h$ to NBP across different timescales, as NPP interacts with $R_h$ by changing carbon pools with a lag over time. Four key parameters were estimated using combined carbon pools and carbon fluxes over 1901-2010 as simulated by TRENDY models. The inputs of the Box-Models are annual NPP and carbon flux by fires (Ffire) calculated by TRENDY models. The outputs are annual NBP and $R_h$, or called $NBP_{TRENDY}^{\tau_{fixed}}$ and $R_{h1}$ to be compared with TRENDY.

Here, we briefly describe the Box-Model. We introduced the matrix equation underlying the carbon-pool-based box model including the effect of disturbances,

which is based on mass balance in carbon processes of terrestrial ecosystem (Luo *et al.*, 2003):

$$\frac{\mathrm{d}C(t)}{\mathrm{d}t} = \xi A C(t) + B u(t) - F v(t) \quad (8)$$

where **C** is a vector of carbon pool sizes. **A** is a transfer matrix, in other words it represents the fractions of carbon transferred from one pool size to the others. $\xi$ is an environmental scalar describing effects of soil temperature and moisture. *u* is a scalar corresponding to the input of carbon fixed by plant photosynthesis over time t. **B** is a vector of fractions of plant photosynthetic carbon allocated to the plant pools. *v* is a scalar corresponding to the release of disturbances (wildfires, land-use change) over time *t*. **F** is a vector of fractions of disturbance emissions released from the carbon pools, and we assume that the release of disturbances is all from the plant pools. The representation of the carbon pools is substantially simpler in this box model compared to the terrestrial ecosystem models in the TRENDY ensemble. To illustrate this, we compared the box model with the land surface model CABLE: all TRENDY models have the same structure but different carbon pool partitioning parameter values. In the sub-model CABLE/CASA-CNP that describes the carbon presses in model (Fig. S4a), there are 9 carbon pool sizes corresponding to leaf, wood, root, metabolic litter, structural litter, coarse woody debris (CWD), fast soil organic matter (SOM), slow SOM, and passive SOM, respectively. In the box model, for simplicity, we reduced these to three carbon pools (Fig. S4b): a plant pool (leaf, wood, and root), a litter pool (metabolic and structural litter, CWD) and a soil pool (fast, slow and passive SOMs). The annual outputs (NPP, $R_h$, NBP, disturbances, 9 carbon pools) of the historical simulation over 1901-2010 by CABLE were used as input to the box model (Eq. **S20**), to estimate annual parameters (e.g. **A**, **B**) of the box model, then the mean of 110-yr annual parameters were used to build the box model (Fig. S4b). For the three-pool box model, according to **Eq. 8**, we have $C=(C_1, C_2, C_3)'$, $B=(b,0,0)'$, $F=(1,0,0)'$, and $A=\begin{pmatrix} 0 & 0 & 0 \\ a_{21} & -a_{22} & 0 \\ 0 & a_{32} & -a_{33} \end{pmatrix}$, then

$$\begin{cases} \dfrac{\mathrm{d}C_1(t)}{\mathrm{d}t} = -a_{21}C_1(t) + bu(t) - v(t) \\ \dfrac{\mathrm{d}C_2(t)}{\mathrm{d}t} = a_{21}C_1(t) - a_{32}C_2(t) - a_{22}C_2(t) \\ \dfrac{\mathrm{d}C_3(t)}{\mathrm{d}t} = a_{32}C_2(t) - a_{33}C_3(t) \end{cases} \quad (9)$$

Using the annual output (C pools, NPP and $R_h$) of CABLE simulations over 1901-2010 as input, that is

$$\begin{aligned} \mathrm{C}(t) &= (C_1(t), C_2(t), C_3(t))' \\ &= (C_{Plant}(t), C_{Litter}(t), C_{Soil}(t))' \end{aligned} \quad (10)$$

$$NPP(t) = bu(t) \quad (11)$$

$$Rh(t) = a_{22}C_2(t) + a_{33}C_3(t) \quad (12)$$

$$NBP(t) = \frac{\mathrm{d}[\mathrm{C}_1(t) + C_2(t) + C_3(t)]}{\mathrm{d}t} \quad (13)$$

we calculated the annual parameters ($a_{21}$, $a_{22}$, $a_{32}$, and $a_{33}$) and the 110-yr averaged parameters ($\overline{a_{21}}$, $\overline{a_{22}}$, $\overline{a_{32}}$, and $\overline{a_{33}}$). Using these four averaged parameters values as optimized parameters, we built the three-pool box-model (Box-Model) that can produce annual NBP and $R_h$ using NPP as input. In this way, the box model was fitted to the output of CABLE.

Following the above procedure, the box model was fitted to the output of each of the TRENDY DGVM models: this produced an ensemble of 10 separate box models. As each of the TRENDY models uses different number of the carbon pools, we combined them into the three pools (plant pool, litter pool, soil pool, some do not have litter pool). Thus, the output annual NBP, $R_h$ and turnover rates as estimated by the box models can be compared to the corresponding original outputs of TRENDY models. All the timeseries of the outputs (i.e. NBP, NPP, $R_h$) from TRENDY models and box models were detrended for comparison of their variability (e.g. NBP in Fig. S5).

**Fractional simulations experiment using the land model CABLE**

Using the land surface model CABLE version 2 (Wang *et al.*, 2010, Wang *et al.*, 2011), we performed a group of fractional simulations in order to attribute variability of NBP, NPP and $R_h$ in response to individual external forcings: $CO_2$ concentration, nitrogen deposition, and seven climate drivers (temperature, precipitation, downward shortwave radiation, downward longwave radiation, humidity, pressure and wind speed). The seven climate drivers were taken from the CRUNCEP version 5 dataset (New *et al.*, 2002) which was used in the TRENDY project in this study. The CRUNCEP data were interpolated to hourly temporal resolution for driving CABLE using cubic splines (Watson, 1992). The annual mean of global surface $CO_2$ concentration during 1901–2010 was used to drive global land grid cells of CABLE in each year; these data were reconstructed from the combination of ice core records in the Antarctic and atmospheric observations since the late 1950s (Keeling & Whorf, 2005). In CABLE, for 110-year simulations, the canopy leaf area index was dynamically predicted (rather than being prescribed). The experiment simulated not only the carbon cycle but also the nitrogen (N) and phosphorous (P) cycles, thus accounting for reduced plant productivity due to possible limitations in N or P (Wang *et al.*, 2010). The significant influence of both N and P limitation for accurately representing biogeochemical cycles in CABLE has been discussed previously, showing that the N limitation would significantly reduce the response of land carbon uptake to the elevated $CO_2$ and the response of carbon loss due to climate changes (Wang *et al.*, 2015, Zhang *et al.*, 2011). In a sensitivity study, we evaluated the effect of nitrogen deposition on the variability in NBP. The annual nitrogen deposition forcing was taken from the ACCMIP dataset over 1901-2010 (Lamarque *et al.*, 2013). Land use change and disturbances (e.g. fires) were not represented in the CABLE simulations. The detailed description of these fractional simulations is listed in Table S2. All simulations were started by the same initial conditions, which were calculated from a 1,000-yr spin-up using a semi-analytical solution method to accelerate the convergence towards a steady state of coupled carbon-nitrogen-phosphorus processes (Xia *et al.*, 2012).

**Spectral analysis for attribution of NBP variation**

We applied spectral analysis to all NBP or NPP and $R_h$ at a global scale or regional scales or at each 0.5° × 0.5° grid-cell across all frequencies (0.01-0.5 $yr^{-1}$) as

estimated by the GCP, TRENDY DGVMs, Box-Models and CABLE fractional simulation experiment. Spectra of these carbon fluxes were calculated for each of the TRENDY models, then spectra ensemble mean were calculated for comparisons. To help identify timescale-dependent drivers, time domain was further divided into three main timescale intervals: inter-annual (2 to 10 years), decadal (10 to 30 years) and multi-decadal (>30 years). In each timescale interval, the variances of all carbon fluxes were integrated with frequency (note that frequency interval varies with study period). The motivation for the summation is that the integral of the power spectrum is equal to the total variance, so the partial integral across a frequency range represents the variance attributable to oscillations at those time-scales. Power spectra of climate variables (i.e. temperature, precipitation etc.) and climate modes ENSO and PDO were also calculated at global or regional scales to help identify the dominant regions or drivers of NBP variations at different timescales. The Fast Fourier Transformation (FFT) filtering algorithm was applied to carbon fluxes and climate variables and climate modes (Fig. S13) to help identifying climate modes modulated regions and the dominant regions and drivers of NBP variation at timescales responding to the characteristic period of climate modes ENSO (2-7 years) and PDO (25-50 years).

## RESULTS

### Attribution of global NBP variation to NPP and $R_h$ across different timescales

Spectral analysis of the observation-based global land carbon sink - hereafter excluding land use change emissions – from the global carbon project (GCP) (Le Quéré *et al.*, 2014) in Figure 1a shows two peaks at frequencies of 0.4 $yr^{-1}$ (once every 2.5 years) and 0.25 $yr^{-1}$ (once every 4 years). The atmospheric $CO_2$ growth rate (Keeling & Whorf, 2005) minus $CO_2$ emissions from fossil fuels and cement (Boden *et al.*, 2016) and land use change emission (Houghton *et al.*, 2012) over 1959-2013 is found peak at the same frequencies as the GCP land carbon sink, revealing that the inter-annual to multi-decadal variability of atmospheric $CO_2$ growth rate was dominated by global terrestrial ecosystems. The independent land carbon sink estimate of CAMS inversion also shows a similar spectra distribution and peaks at the same frequencies as the GCP land carbon sink (Figure 1a). The LULCC contributes relative small variances at the low frequencies (periods of 10-30 years), and fires

emission shows negligible variances over all frequencies compared to the GCP residual sink (Figure 1a). Overall, multiple sources of carbon fluxes reveal that the global carbon cycle is mostly dominated by the land carbon sink, basically the global terrestrial ecosystems.

To analyze the variation of global land NBP and contributions of its components (NNP, $R_h$) at different time scales, we used these fluxes of the 110-year simulations from ten DGVMs forced by historical climate and $CO_2$ (Piao *et al.*, 2013) as the models are capable to reproduce observed inter-annual variations and decadal mean values of the land sink (Le Quéré *et al.*, 2014). Figure 1b shows that the variance spectrum of global $NBP_{TRENDY}$ averaged across all the models has two peaks at frequencies of 0.4 $yr^{-1}$ (once every 2-3 years) and 0.28 $yr^{-1}$ (once every 3.57 years), close to the observed modes of variability in Figure 1a. The TRENDY models also produced a lower frequency peak at 0.03 $yr^{-1}$ (once every 33.3 years) (Figure 1b) which is consistent with the CAMS inversion and the GCP. The difference in the variance spectrum between $NBP_{TRENDY}$ and $NBP^{\tau_{fixed}}_{TRENDY}$ represents the variations of global NBP due to variable decomposition rates alone ($R_{h2}$). As shown in Figure 1b, the differences in the variance spectrum between $NBP_{TRENDY}$ and $NBP^{\tau_{fixed}}_{TRENDY}$ are much larger at the timescales of 30-100 years (or frequencies 0.01-0.03 $yr^{-1}$) than that at shorter timescales, suggesting a relatively larger contribution from $R_{h2}$ to the multi-decadal NBP variations.

To analyze the time-scale dependence of the variance contributions of NPP and $R_h$ to NBP, we identified three time scales: inter-annual (2 to 10 years), decadal (10 to 30 years) and multi-decadal (>30 years) based on the spectral characteristics of both observed land carbon sinks and modeled NBP variations (see Figures 1a-b); and integrated variance spectra of NBP, NPP and $R_h$ over the three different frequency intervals. The GCP residual sink shows close integrated variances to the natural atmospheric $CO_2$ growth rate with about 0.7-0.75 $(Pg\ C)^2yr^{-2}$ at inter-annual timescales, about 0.15 $(Pg\ C)^2yr^{-2}$ at decadal timescales and about 0.13 $(Pg\ C)^2yr^{-2}$ at multi-decadal timescales (Figure 1c). The CAMS land sink that was calculated from 38-year time series shows lower variances at inter-annual timescales (0.65 $(Pg\ C)^2yr^{-2}$) and higher at decadal timescales (0.25 $(Pg\ C)^2yr^{-2}$) than the GCP estimates. The TRENDY modeled NBP is in good agreement with the GCP and the CAMS with 0.8±0.15 $(Pg\ C)^2yr^{-2}$ at inter-annual timescales, 0.15±0.10 $(Pg\ C)^2yr^{-2}$ at decadal

timescales, and 0.13±0.05 (Pg C)$^2$yr$^{-2}$ at inter-annual timescales (Figure 1c). Both the GFED4 fires emission and the TRENDY modeled D (fires) show small variance at inter-annual timescales (0.05±0.05 (Pg C)$^2$yr$^{-2}$) and negligible variance (~0.01 (Pg C)$^2$yr$^{-2}$) at decadal timescales.

The total variance of $NBP_{TRENDY}$ is dominated by the inter-annual timescales of 2-10 years (72%), with non-negligible contributions from the decadal timescales of 10-30 years (15%) and multi-decadal timescales of 30-100 years (13%) (Figure 1c). At inter-annual timescale, the variance of NBP constitute 86% of the variance of NPP, and the variance of $R_{h1}$ and $R_{h2}$ only constitute 1% and 21% of the variance of NPP (Figure 1c). In other words, NPP dominates the inter-annual variance of global NBP, as given by the solution of Equations 5-6 fitted to TRENDY models (Fig. S1). The variance of $R_{h2}$ dominates the variance of $R_h$ (96%) at inter-annual timescale, indicating that climate-driven fluctuations of carbon decomposition turnover rates ($R_{h2}$) rather than NPP-driven variable carbon input to soils ($R_{h1}$) dominates the inter-annual variability of $R_h$ (Figure 1c).

At decadal timescales, the variance of the modeled NPP ensemble is smaller than that at inter-annual or multi-decadal timescales (Figure 1c). The ratio of the variance of NBP to that of NPP from equation (5) decreases from 86% at inter-annual timescale down to 20% at multi-decadal timescale. Conversely, the ratio of the variance of $R_h$ to that of NPP increases with longer timescales, is consistent with the theoretical prediction of an increasing importance of $R_h$ variations for the slow changes in the carbon cycle (Fig. S1). The variance of $R_{h2}$ by variable soil carbon turnover rates dominates the variance of $R_h$ at decadal timescales (Figure 1c) and explains 60% of the variance of $R_h$ at multi-decadal timescales. Overall, the variability of $R_h$ at the multi-decadal timescale is jointly controlled by the slow variability of NPP (40%) and by the component of $R_h$ due to variable decomposition rates (60%).

**Attribution of regional NBP variations to NPP and $R_h$ at different timescales**

To identify the regions that dominate the variability of NBP in the TRENDY models and land sinks from CAMS inversion, we considered 11 regions as in previous studies (Gurney *et al.*, 2002, Peylin *et al.*, 2013) (see Supplementary Materials, Fig. S6a, Table S3) and calculated spectra of modeled NBP ensemble mean and CAMS inverted land sink for all regions. Among the 11 regions, multi-model

averagely, the variance of regional modeled NBP is dominated by inter-annual (2-10 years, 48% to 82%), followed by decadal (10-30 years, 11% to 26%) and multi-decadal (30-100 years, 7% to 28%) timescales (Figure 2). By integrating variance across all timescales, we found that tropical South America (or the Amazonia rainforest) is the largest contributor (32%) to the variance of global modeled NBP ensemble, followed by Southern Africa (13%), temperate North America (10%), and other regions (less than 10%).

At inter-annual timescales, the TRENDY modeled results show that tropical South America accounts for the largest contribution (19%) of the total global modeled NBP variance, followed by Southern Africa (14%), temperate North America (13%), and temperate South America (11%). While the CAMS inversion shows that the Southern Africa (18%) is the largest contributor of global land sink inter-annual variance, followed by tropical South America (14%), temperate North America (14%), and Europe (14%).

At decadal timescales, both TRENDY models ensemble and CAMS shows that tropical South America is the dominant region accounting for 24% of the global decadal integrated variance (Figure 2), followed by Southern Africa (17%). At multi-decadal timescales in the TRENDY models, tropical South America clearly dominates as it explains 51% of global NBP variance, whereas the second most influential region Southern Africa explains only 10%. Note that multi-decadal variance could be estimated by CAMS because of its only 38-year land sink time series. Therefore we find that tropical South America is the dominant contributor to global NBP variation at all timescales in TREDNY models ensemble and at decadal timescales in CAMS, which differs from the conclusion that the inter-annual variability and trend of global NBP are mainly caused by semi-arid regions in Ahlström et al. (Ahlström *et al.*, 2015). This inconsistence may result from the different regions defined between this study and Ahlström et al. (Ahlström *et al.*, 2015) and/or be too short study periods (~30 years) in Ahlström et al. (Ahlström *et al.*, 2015) to elucidate multi-decadal variability of global NBP. To clarify this issue, we grouped the global land ecosystems into six land cover classes (e.g. tropical rainforests, extra-tropical forests, semi-arid ecosystems, and grasslands and croplands etc.) as defined by Ahlström et al. (Ahlström *et al.*, 2015) (Fig. S6b, Table S4), we find that the dominant contributors to the variability of global NBP are tropical rainforests (48%) rather than semi-arid ecosystems (35%) at multi-decadal timescales based on estimate of TRENDY models.

We also reveal that the semi-arid regions are the largest contributors to the global NBP variations both at the inter-annual (49% for TRENDY and 60% for CAMS) and decadal timescales (46% for TRENDY and 52% for CAMS), which is consistent with Ahlström et al. (Ahlström *et al.*, 2015) (Table S4). The semi-arid ecosystems consist of ~25% of the global vegetated land area, and tropical rainforests only occupy 11% (Table 1). We normalized the contributions by per unit of land area and further find that tropical rainforests per land area contribute 1.1 (or 0.7) and 1.4 (or 0.9) times to modelled NBP (or CAMS land sink) variance at inter-annual and decadal timescales respectively than that of the semi-arid ecosystems per land area (Table 1). But at multi-decadal timescales, tropical rainforests contribute 3.1 times of variance than that in the semi-arid ecosystems at per unit land area (Table 1). This reveals that tropical rainforests have the potential to control the variability of global NBP than semi-arid ecosystems over multi-decadal timescales. Therefore, we suggest that tropical rainforests are the dominator of the multi-decadal variability of the global carbon cycle.

Compared to TRENDY models ensemble at regional scales, the CAMS land sink shows generally consistent patterns for Tropical South America and Tropical Asia (Figure 3a-b), yet has larger by at least 50% of variance contributions for Temperate South America, Northern Africa, Southern Africa and Europe across all timescales (Figure 3d-f and 3i) than TRENDY modelled NBP. In Australia, the CAMS has negligible variances at all timescales largely that disagrees with TRENDY (Figure 3c). The modelled fire emissions at regional scales are consistent with the estimate of GFED4 except the Tropical Asia region where GFED4 includes large contributions of annual emissions from peat land and man-made fires (Giglio *et al.*, 2013).

Contributions of NPP and $R_h$ to regional NBP variations in TRENDY models show general patterns across the timescales, although they vary with different regions. In general, variance of NPP dominates the variation of NBP at inter-annual time scale (Figure 3), and that dominance decreases with an increase in time scale, as supported by the ratio of the variance of NBP to that of NPP decreases with an increase in time scale (Fig. S1). The variance of $R_h$ is larger at multi-decadal timescale than that at inter-annual timescale. The increasing importance of $R_{h1}$ to the variance of $R_h$ with an increase in timescale is particularly significant in tropical and temperate regions. At multi-decadal timescale, $R_{h1}$ dominates $R_h$ in these regions. This suggests that variations of NBP due to variations of NPP could be dampened by turnover in the

carbon cycle system at multi-decadal timescale in tropical and temperate regions. However, $R_{h2}$ still dominates ~99% of variance of $R_h$ in Australia, Northern Africa and boreal regions (Figure 3), as a result of relatively longer residence time of ecosystem carbon in these regions.

**The dominant drivers of regional NBP variations at short and long timescales**

The global NBP variance clearly peaks at 2.5-7 years and 25-50 years timescales (Figure 1a-b). Hence, we focus on identifying the key drivers of NBP variance at these two timescales. By analysing the results from a full factorial simulations using the DGVM CABLE version 2, we identified that temperature, precipitation are the most important drivers of global NBP variations at all timescales, and that $CO_2$ concentration is important for NBP components NPP and $R_h$ on long timescales (Fig. S7). But their relative importance varies across different regions (Figure 4). Several notable peaks of variance in modeled NBP power spectra are caused by the variations of surface air temperature and/or precipitation in tropical and semi-arid regions (Figure 4). The NBP variance at inter-annual to decadal timescales mainly results from variation of NPP driven by variations of temperature and precipitation (Figs. S7b and S8), rather than variation of $R_h$ (Figs. S7c and S9). This suggests that NBP variances in these regions at the timescales of 2.5-7 years and 25-50 years are closely linked to large-scale climate oscillations of ENSO and PDO via climate variability (Fig. S10).

At the short timescale of ENSO-like cycles of 2.5-7 years, the $NBP_{TRENDY}$ in tropical South America and Asia, Africa and Australia are significantly and negatively correlated with the ENSO ($R=-0.35$ to $-0.66$, $P<0.01$) and these regions contribute ~60% of the global NBP variance (Figure 5a). Tropical South America as the largest contributors for global variance of NBP (Figure 5a), has significant correlations between ENSO index and the surface air temperature ($R=0.73$, $P<0.001$) and precipitation ($R=-0.74$, $P<0.001$) (Figure 5c), which regulating variation of NBP via NPP in that region at the short timescale (Fig. S11).

At the long timescale of PDO cycles (25-50 years), tropical South America contributes about 50% of the global NBP variance and is significantly and negatively correlated with the PDO index ($R=-0.80$, $P<0.001$) (Figure 5b). This can be attributed to that the PDO index negatively correlates with NPP via regulating temperature and

in tropical South America (Figure 5d and Fig. S11). Contribution to the global NBP variance from each of other region is less than 10% at the long timescale (Figure 5b).

## DISCUSSION

Which regions dominate the inter-annual or multi-decadal variability of global NBP? In this study, we find that the answer to this question depends on how the land regions (area) are defined and on which timescales. We compared the results with the definitions of land cover classes from Ahlström et al. (Ahlström *et al.*, 2015), and also revealed that semi-arid ecosystems dominate the inter-annual variability of global NBP from both TRENDY models and CAMS inversion estimates. However, our results indicate that tropical rainforests rather than semi-arid ecosystems dominate the multi-decadal variability of global NBP and therefore the growth rate of atmospheric $CO_2$. Tropical rainforests shows larger efficiency for carbon sequestration on long timescales. This suggests that more efforts are needed to make on the worldwide tropical rainforests conservation and reforestations for climate mitigation in the future.

Both NPP and carbon residence have been proposed to be the dominant contributor to global NBP variation (Friend *et al.*, 2014, Matthews *et al.*, 2005). Using the theory we developed to the output of TRENDY models, we show that NPP variation mainly dominate NBP variation both globally and regionally at inter-annual timescales, but the NPP contribution decreases with an increase of timescale. By contrast, the contribution of $R_h$ to the NBP variations increases with an increase of timescale. Furthermore, we find that the two components of $R_h$ variations, NPP-driven ($R_{h1}$) and turnover rate induced ($R_{h2}$) variations, contribute to NBP variation differently. Variation of $R_{h1}$ driven by NPP contributes negatively to the variation of NBP, i.e. more NPP causes more soil carbon and then more respiration that attenuates the response of NBP to NPP, and $R_{h1}$ progressively contribute more over longer timescales (Figure 1c). By contrast, the variability of $R_{h2}$ may offset or amplify the variability of NBP relative to NPP depending on whether climate anomalies impact NPP vs. decomposition turnover rates in an additive or subtractive manner. The increasing role of $R_{h2}$ in controlling the variability of NBP with increasing timescale (Figures 1 and 3; Fig. S1) implies that fluctuations in ecosystem carbon turnover rates play a significant role in reducing variations of NBP. Therefore, without

differentiating different time scales may lead to erroneous conclusion of the dominant control of NBP variation at a long time scale.

The climate modes have been found to significantly modulate the regional NBP variations at inter-annual and multi-decadal timescales (Bastos *et al.*, 2013, Betts *et al.*, 2016, Wang *et al.*, 2013, Zeng *et al.*, 2005). Climate inter-annual oscillations ENSO (2.5-7 years) and decadal to multi-decadal oscillations PDO (25-50 years) can strongly influence precipitation and temperature in tropical forests (Tian *et al.*, 1998, Wang *et al.*, 2013), and semi-arid regions in Africa (Dong & Dai, 2015), North America (Khedun *et al.*, 2014) and Australia (Power *et al.*, 1999). ENSO-regulated variations of temperature and precipitation controls the variations of global NBP at inter-annual timescale (Wang *et al.*, 2013, Zeng *et al.*, 2005), and trends of temperature, precipitation and $CO_2$ concentration that contribute to the trends of global NBP (Keenan *et al.*, 2016, Schimel *et al.*, 2015). In this study, based on multi-models diagnostic analysis, we found that higher (lower) temperature and less (more) precipitation during ENSO cycles induce larger variability of NPP, $R_h$ and NBP in tropical forests and semi-arid regions at inter-annual timescales (Figure 5). In a warmer world, both the frequency and magnitude of El Niño events, especially drying driven by El Niño events, is projected to be intensified (Cai *et al.*, 2014) which intensify the variability of NBP in these regions and increase their contribution to global NBP variation.

At decadal to multi-decadal timescales, our modeling results show that PDO cycles can strongly regulate the global and tropical terrestrial NBP via the controls of surface air temperature and precipitation on the variability of NPP and $R_h$ (Figure 5). The shifts in PDO phase responsible for shifts in rainfall regime in 1945–46 and in 1975–77 (Meehl *et al.*, 2009), are found to link with the shift of temperature and precipitation regime in tropical South America and Australia (Power *et al.*, 1999, Power *et al.*, 2013). These two shifts of PDO phase are also found to control NBP variation at multi-decadal timescales in tropical South America and Australia through NPP and $R_h$ (Fig. S11). The trend in NBP in semi-arid regions during the last three decades may be related to the influences of a positive phase of the PDO after 1976 (Power *et al.*, 1999), and may not last long into the future if PDO goes into negative phase. In addition, Woodward et al. (Woodward *et al.*, 2008) indicated that the sensitivities of precipitation and production of vegetation to ENSO index are stronger in a cool phase of PDO (1951-1976) than that in a warm phase of PDO (1976-2002).

This implies that the superimposed ENSO on cool phase of PDO may further enlarge the variability of NBP in the next decades.

This study calls for analysis of the factors controlling decadal or longer timescale fluctuations in NBP with long-term carbon fluxes observation to gain insights on the future evolution of the global land carbon sink. Long-term observations of NPP, $R_h$ and NBP and longer periods of and carbon sink inversion products are needed to verify their variability at different timescales and different regions. Well-designed manipulative experiments, such as estimating changes in plant litter pool and soil organic carbon pool, could also help to distinguish the contribution of NPP, $R_{h1}$ and $R_{h2}$ on NBP.

Although DGVMs multi-model ensemble may help represent terrestrial carbon cycling (Le Quéré *et al.*, 2013), the process-based DGVMs have uncertainties in GPP parameterizations that may result in over/under estimating GPP (or NPP) inter-annual variability. The comparison of TRENDY GPP with observation-based GPP from CARDAMOM, MODIS and FLUXCOM (Figs. S14-S15) shows that TRENDY GPP is comparable with observations and quiet similar to FLUXCOM for the tropical rainforest, semi-arid and other regions (Fig. S15) revealing that larger inter-annual variability in semi-arid ecosystems than tropical rainforests. Furthermore, the relative importance of the variability of regional NBP to the variability of global NBP depends on the carbon turnover rate of ecosystem in TRENDY DGVMs, which may have bias regionally in this study compared with the CARDMOM estimate (Fig. S12). TRENDY DGVMs shows higher (lower) turnover rates in temperate and boreal ecosystems (tropical rainforests) than CARDAMOM. The bias in turnover rates reflects uncertainties of representations within DGVMs' ecosystem carbon cycle processes such as photosynthesis parameterization, plant carbon allocation, nutrient limitation effect, and simple soil carbon decomposition schemes (Wang *et al.*, 2017, Wieder *et al.*, 2013). Since carbon turnover time of ecosystems in boreal regions is much longer than 100 years (Bloom *et al.*, 2016, Erb *et al.*, 2016), the contribution of variability of NBP in boreal regions to global NBP at timescales longer than 100 years may stand out from other regions. Paleoclimate records, as well as long-term simulations at centurial or millennial or even longer timescales, could help to understand the variability of NBP and changes in turnover times due to climate change at timescales longer than 100 years.

**Acknowledgements**

This study was founded by National Key Research and Development Program of China (2016YFA0600202 and 2016YFC0500203), and National Natural Science Foundation of China (41722101). X. Zhang was also partially supported by the China Postdoctoral Science Foundation (2016M600853). Y. W. was supported by the CSIRO and Chinese Academy of Sciences' strategic funding on global terrestrial biogeochemistry. P. R. was partly supported by an Australian Professorial Fellowship (DP1096309). J. S. was supported by a McKenzie Postdoctoral Fellowship from the University of Melbourne. P. C. acknowledges support from the European Research Council Synergy grant ERC-2013-SyG-610028 IMBALANCE-P. We acknowledge participants of the TRENDY model inter-comparison project for access to their simulation results. This study was also undertaken with the assistance of resources from the National Computational Infrastructure (NCI), which is supported by the Australian Government.

**Conflict of Interest** The authors declare no competing financial interests.



## REFERENCES

Ahlström A, Raupach MR, Schurgers G *et al.* (2015) Carbon cycle. The dominant role of semi-arid ecosystems in the trend and variability of the land CO2 sink. Science, **348**, 895-899.

Anderegg WR, Ballantyne AP, Smith WK *et al.* (2015) Tropical nighttime warming as a dominant driver of variability in the terrestrial carbon sink. Proc Natl Acad Sci U S A, **112**, 15591-15596.

Bastos A, Running SW, Gouveia C, Trigo RM (2013) The global NPP dependence on ENSO: La Niña and the extraordinary year of 2011. Journal of Geophysical Research: Biogeosciences, n/a-n/a.

Betts RA, Jones CD, Knight JR, Keeling RF, Kennedy JJ (2016) El Niño and a record CO2 rise. Nature Climate Change, **6**, 806-810.

Bloom AA, Exbrayat JF, Van Der Velde IR, Feng L, Williams M (2016) The decadal state of the terrestrial carbon cycle: Global retrievals of terrestrial carbon

allocation, pools, and residence times. Proc Natl Acad Sci U S A, **113**, 1285-1290.

Bloom AA, Williams M (2015) Constraining ecosystem carbon dynamics in a data-limited world: integrating ecological "common sense" in a model–data fusion framework. Biogeosciences, **12**, 1299-1315.

Boden TA, Marland G, Andres RJ (2016) *Global, Regional, and National Fossil-Fuel CO2 Emissions,* Carbon Dioxide Information Analysis Center, Oak Ridge National Laboratory, U.S. Department of Energy, Oak Ridge, Tenn., U.S.A.

Cai W, Borlace S, Lengaigne M *et al.* (2014) Increasing frequency of extreme El Niño events due to greenhouse warming. Nature Climate Change, **4**, 111-116.

Chevallier F, Ciais P, Conway TJ *et al.* (2010) CO2 surface fluxes at grid point scale estimated from a global 21 year reanalysis of atmospheric measurements. Journal of Geophysical Research, **115**.

Cox PM, Pearson D, Booth BB, Friedlingstein P, Huntingford C, Jones CD, Luke CM (2013) Sensitivity of tropical carbon to climate change constrained by carbon dioxide variability. Nature, **494**, 341-344.

Dong B, Dai AG (2015) The influence of the Interdecadal Pacific Oscillation on Temperature and Precipitation over the Globe. Climate Dynamics, **45**, 2667-2681.

Erb K-H, Fetzel T, Plutzar C *et al.* (2016) Biomass turnover time in terrestrial ecosystems halved by land use. Nature Geoscience, **9**, 674-678.

Forkel M, Carvalhais N, Rodenbeck C *et al.* (2016) Enhanced seasonal CO2 exchange caused by amplified plant productivity in northern ecosystems. Science, **351**, 696-699.

Friend AD, Lucht W, Rademacher TT *et al.* (2014) Carbon residence time dominates uncertainty in terrestrial vegetation responses to future climate and atmospheric CO2. Proc Natl Acad Sci U S A, **111**, 3280-3285.

Giglio L, Randerson JT, Van Der Werf GR (2013) Analysis of daily, monthly, and annual burned area using the fourth-generation global fire emissions database (GFED4). Journal of Geophysical Research: Biogeosciences, **118**, 317-328.

Graven HD, Keeling RF, Piper SC *et al.* (2013) Enhanced seasonal exchange of CO2 by northern ecosystems since 1960. Science, **341**, 1085-1089.

Gurney KR, Baker D, Rayner P, Denning S (2008) Interannual variations in continental-scale net carbon exchange and sensitivity to observing networks

estimated from atmospheric CO2 inversions for the period 1980 to 2005. GLOBAL BIOGEOCHEMICAL CYCLES, **22**, GB3025.

Gurney KR, Law RM, Denning AS *et al.* (2002) Towards robust regional estimates of CO2 sources and sinks using atmospheric transport models. Nature, **415**, 626-630.

Hantson S, Arneth A, Harrison SP *et al.* (2016) The status and challenge of global fire modelling. Biogeosciences, **13**, 3359-3375.

Houghton RA, House JI, Pongratz J *et al.* (2012) Carbon emissions from land use and land-cover change. Biogeosciences, **9**, 5125-5142.

Houghton RA, Nassikas AA (2017) Global and regional fluxes of carbon from land use and land cover change 1850-2015. GLOBAL BIOGEOCHEMICAL CYCLES, **31**, 456-472.

Jacobson AR, Mikaloff Fletcher SE, Gruber N, Sarmiento JL, Gloor M (2007) A joint atmosphere-ocean inversion for surface fluxes of carbon dioxide: 2. Regional results. GLOBAL BIOGEOCHEMICAL CYCLES, **21**, GB1020.

Jung M, Reichstein M, Schwalm CR *et al.* (2017) Compensatory water effects link yearly global land CO2 sink changes to temperature. Nature, **541**, 516-520.

Kalnay E, Kanamitsu M, Kistler R *et al.* (1996) The NCEP/NCAR 40-Year Reanalysis Project. Bulletin of the American Meteorological Society, **77**, 437-471.

Keeling CD, Whorf TP (2005) Atmospheric CO2 records from sites in the SIO air sampling network, trends : a compendium of data on global change. Oak Ridge National Laboratory, US Department of Energy, USA : Carbon Dioxide Information Analysis Center.

Keenan TF, Prentice IC, Canadell JG, Williams CA, Wang H, Raupach M, Collatz GJ (2016) Recent pause in the growth rate of atmospheric CO2 due to enhanced terrestrial carbon uptake. Nat Commun, **7**, 13428.

Khedun CP, Mishra AK, Singh VP, Giardino JR (2014) A copula-based precipitation forecasting model: Investigating the interdecadal modulation of ENSO's impacts on monthly precipitation. Water Resources Research, **50**, 580-600.

Lamarque JF, Dentener F, Mcconnell J *et al.* (2013) Multi-model mean nitrogen and sulfur deposition from the Atmospheric Chemistry and Climate Model Intercomparison Project (ACCMIP): evaluation of historical and projected future changes. Atmospheric Chemistry and Physics, **13**, 7997-8018.

Le Quéré C, Peters GP, Andres RJ *et al.* (2014) Global carbon budget 2013. Earth System Science Data, **6**, 235-263.

Le Quéré C, Raupach MR, Canadell JG *et al.* (2009) Trends in the sources and sinks of carbon dioxide. Nature Geoscience, **2**, 831-836.

Liu J, Bowman KW, Schimel DS *et al.* (2017) Contrasting carbon cycle responses of the tropical continents to the 2015-2016 El Nino. Science, **358**.

Luo Y, White LW, Canadell JG *et al.* (2003) Sustainability of terrestrial carbon sequestration: A case study in Duke Forest with inversion approach. GLOBAL BIOGEOCHEMICAL CYCLES, **17**, 1-13.

Matthews HD, Eby M, Weaver AJ, Hawkins BJ (2005) Primary productivity control of simulated carbon cycle-climate feedbacks. Geophysical Research Letters, **32**, n/a-n/a.

Meehl GA, Hu AX, Santer BD (2009) The Mid-1970s Climate Shift in the Pacific and the Relative Roles of Forced versus Inherent Decadal Variability. Journal of Climate, **22**, 780-792.

Mitchell TD, Jones PD (2005) An improved method of constructing a database of monthly climate observations and associated high-resolution grids. International Journal of Climatology, **25**, 693-712.

New M, Lister D, Hulme M, Makin I (2002) A high-resolution data set of surface climate over global land areas. Climate Research, **21**, 1-25.

Pan Y, Birdsey RA, Fang J *et al.* (2011) A large and persistent carbon sink in the world's forests. Science, **333**, 988-993.

Peylin P, Law RM, Gurney KR *et al.* (2013) Global atmospheric carbon budget: results from an ensemble of atmospheric CO2 inversions. Biogeosciences, **10**, 6699-6720.

Piao S, Sitch S, Ciais P *et al.* (2013) Evaluation of terrestrial carbon cycle models for their response to climate variability and to CO2 trends. Glob Chang Biol, **19**, 2117-2132.

Poulter B, Frank D, Ciais P *et al.* (2014) Contribution of semi-arid ecosystems to interannual variability of the global carbon cycle. Nature, **509**, 600-603.

Power S, Casey T, Folland C, Colman A, Mehta V (1999) Inter-decadal modulation of the impact of ENSO on Australia. Climate Dynamics, **15**, 319-324.

Power S, Delage F, Chung C, Kociuba G, Keay K (2013) Robust twenty-first-century projections of El Nino and related precipitation variability. Nature, **502**, 541-545.

Schimel D (2007) Carbon cycle conundrums. Proc Natl Acad Sci U S A, **104**, 18353-18354.

Schimel D, Stephens BB, Fisher JB (2015) Effect of increasing CO2 on the terrestrial carbon cycle. Proc Natl Acad Sci U S A, **112**, 436-441.

Shevliakova E, Stouffer RJ, Malyshev S, Krasting JP, Hurtt GC, Pacala SW (2013) Historical warming reduced due to enhanced land carbon uptake. Proc Natl Acad Sci U S A, **110**, 16730-16735.

Sitch S, Friedlingstein P, Gruber N *et al.* (2015) Recent trends and drivers of regional sources and sinks of carbon dioxide. Biogeosciences, **12**, 653-679.

Thomson RE, Emery WJ (2014) *Data Analysis Methods in Physical Oceanography (Third Edition)*, Elsevier Science.

Tian H, Melillo JM, Kicklighter DW, Mcguire AD, Helfrich JVK, Moore B, Vörösmarty CJ (1998) Effect of interannual climate variability on carbon storage in Amazonian ecosystems. Nature, **396**, 664-667.

Tubiello FN (2012) *Climate change adaption and mitigation: challenges and opportunities in the food sector*, Natural Management and Environment Department, FAO, Rome, Food and Agriculture Organization of the United Nations (FAO).

Van Der Werf GR, Randerson JT, Giglio L *et al.* (2010) Global fire emissions and the contribution of deforestation, savanna, forest, agricultural, and peat fires (1997–2009). Atmospheric Chemistry and Physics, **10**, 11707-11735.

Wang W, Ciais P, Nemani RR *et al.* (2013) Variations in atmospheric CO2 growth rates coupled with tropical temperature. Proc Natl Acad Sci U S A, **110**, 13061-13066.

Wang Y, Law R, Pak B (2010) A global model of carbon, nitrogen and phosphorus cycles for the terrestrial biosphere. Biogeosciences, **7**.

Wang Y-P, Zhang Q, Pitman AJ, Dai Y (2015) Nitrogen and phosphorous limitation reduces the effects of land use change on land carbon uptake or emission. Environmental Research Letters, **10**, 014001.

Wang YP, Kowalczyk E, Leuning R *et al.* (2011) Diagnosing errors in a land surface model (CABLE) in the time and frequency domains. Journal of Geophysical Research: Biogeosciences (2005–2012), **116**.

Watson DF (1992) *Contouring: A Guide to the Analysis and Display of Spatial Data*, Oxford, Pergamon Press.

Woodward FI, Lomas MR, Quaife T (2008) Global responses of terrestrial productivity to contemporary climatic oscillations. Philos Trans R Soc Lond B Biol Sci, **363**, 2779-2785.

Xia JY, Luo YQ, Wang YP, Weng ES, Hararuk O (2012) A semi-analytical solution to accelerate spin-up of a coupled carbon and nitrogen land model to steady state. Geoscientific Model Development, **5**, 1259-1271.

Zeng N, Mariotti A, Wetzel P (2005) Terrestrial mechanisms of interannual CO2 variability. GLOBAL BIOGEOCHEMICAL CYCLES, **19**, GB1016.

Zhang Q, Wang YP, Pitman AJ, Dai YJ (2011) Limitations of nitrogen and phosphorous on the terrestrial carbon uptake in the 20th century. Geophysical Research Letters, **38**, L22701.

Zhao M, Heinsch FA, Nemani RR, Running SW (2005) Improvements of the MODIS terrestrial gross and net primary production global data set. Remote Sensing of Environment, **95**, 164-176.

Zhao M, Running SW (2010) Drought-induced reduction in global terrestrial net primary production from 2000 through 2009. Science, **329**, 940-943.

**Table 1** Regional contribution (%) per 1% of global land area to variances in global land NBP from TRENDY ensemble and CAMS atmospheric $CO_2$ inversion in six regions at different timescales. Land cover classes were given by Ahlström et al. (Ahlström *et al.*, 2015).

| Region | Area (%) | Data sources | Variance contribution (mean ± σ %) per 1% of global land area | | |
|---|---|---|---|---|---|
| | | | 2-10 yrs | 10-30 yrs | 30-100 yrs |
| Tropical forests | 10.9 | CAMS | 1.70 | 1.83 | — |
| | | TRENDY | 2.19 ± 1.05 | 2.61 ± 2.39 | 4.39 ± 3.55 |
| Extra-tropical forests | 10.4 | CAMS | 0.35 | 0.50 | — |
| | | TRENDY | 0.36 ± 0.16 | 0.27 ± 0.14 | 0.36 ± 0.22 |
| Semi-arid regions | 25.3 | CAMS | 2.38 | 2.09 | — |
| | | TRENDY | 1.94 ± 0.79 | 1.83 ± 1.07 | 1.38 ± 0.83 |
| Grasslands & crops | 29.2 | CAMS | 0.51 | 0.72 | — |
| | | TRENDY | 0.75 ± 0.29 | 0.72 ± 0.39 | 0.37 ± 0.22 |

| | | | | | |
|---|---|---|---|---|---|
| Tundra & arctic shrub | 10.4 | CAMS | 0.56 | 0.23 | — |
| | | TRENDY | 0.13 ± 0.08 | 0.15 ± 0.01 | 0.22 ± 0.13 |
| Sparsely vegetated | 13.9 | CAMS | 0.03 | 0.02 | — |
| | | TRENDY | 0.01 ± 0.01 | 0.01 ± 0.01 | 0.01 ± 0.00 |



## Figure captions

**FIGURE 1 Comparison of variances of carbon fluxes from atmospheric $CO_2$ growth rate excluding anthropogenic emissions, GCP, CAMS $CO_2$ inversion, TRENDY and Box-Models at different timescales.** (a) Spectral analysis for global annual land carbon sink from the Global Carbon Project (GCP) over 1959-2010. Natural atmospheric $CO_2$ growth is defined as the observed atmospheric $CO_2$ growth excluding anthropogenic $CO_2$ emissions. Global land carbon sink from CAMS $CO_2$ inversion covering the period of 1979 to 2016 with fossil emission adjusted, is also used as an independent comparison; (b) Spectral analysis for global annual NBP (mean ± standard deviation (σ)) from ten DGVMs in TRENDY ensemble ($NBP_{TRENDY}$) and from their respective Box-Models ensemble ($NBP^{\tau_{frod}}_{TRENDY}$) across all frequencies over 1901-2010; (c) Comparison of variance of global NBP, NPP, $R_{h1}$, $R_{h2}$ and the other disturbance (D) from ten DGVMs in TRENDY ensemble for inter-annual (2-10 years), decadal (10-30 years) and multi-decadal (30-100 years) timescales respectively. $R_h$ is decomposed into $R_{h1}$ and $R_{h2}$. $R_{h1}$ is defined as NPP-dependent response of $R_h$, which is calculated from the output of the three-pool Box-Models. $R_{h2}$ is the release of heterotrophic respiration due to the climatic response of turnover rate, which is the difference of $R_h$ from TRENDY models and $R_{h1}$ from Box-Models. The dashed lines in Figure 1c donate uncertainties (mean ± σ) for the carbon fluxes.

**FIGURE 2 Contributions of variance of NBP from TRENDY DGVMs and CAMS at global and regional scales at different timescales.** The pie charts over each coloured region represent contributions of inter-annual (2-10 years, in blue), decadal (10-30 years, in red) and multi-decadal (30-100 years, in light green) variances to the variance in NBP of the region. The size of each pie chart for each

region denotes the regional contribution of variance in NBP to the total variance in global NBP. The left lower three piecharts indicate the contributions of variance in NBP of the eleven regions (corresponding to the upper mapping colours) to the variance of global NBP from TRENDY DGVMs at different timescales, and the right lower piecharts are same as the left lower piecharts but for CAMS inversion.

**FIGURE 3 Comparison of variance of carbon fluxes from TRENDY DGVMs ensemble, GFED4 and CAMS for 11 regions at different timescales.** Figure description is the same as Figure 1c, but for eleven land regions. The dashed lines indicate uncertainties (mean ± σ). Emissions of biomass burning from GFED4.1s product over 1997-2016 were used as comparisons to TRENDY modeled D (e.g. fires). Land NBP estimated from CAMS atmospheric $CO_2$ inversion product (version v16r1) over 1979-2016 was also compared to TRENDY modeled NBP regionally across different timescales.

**FIGURE 4 Spectral analysis for annual NBP calculated from fractional simulations of nine external drivers for eleven regions (a-k) over 1901-2010.** The nine fractional simulations are simulated using the DGVM model CABLE version 2.0 forced by varying individual member of nine drivers (atmospheric N deposition, $CO_2$ concentration, temperature, precipitation, short- and long- wave radiations, specific humidity, surface pressure, and wind speed) over 1901-2010, and all others being set at their climatological value. The nine fractional simulations of CABLE experiment are described in Table S2.

**FIGURE 5 Regional NBP from TRENDY DGVMs relates to temperature and precipitation and ENSO or PDO indices.** (a) Relative contributions of variance in regional NBP to the global NBP variance at timescales of 2.5-7 years versus correlation coefficients of regional NBP and ENSO time-series at timescales of 2.5-7 years; (b) same as (a) but for the timescales of 25-50 years versus the correlation coefficients between the regional NBP and the PDO index; (c) Correlations of regional precipitation and temperature with ENSO index at timescales of 2.5-7 years; (d) Correlation coefficients of regional precipitation and temperature with PDO index at timescales of 25-50 years. Here, time-series of NBP, ENSO (SST Nino 3.4 index), PDO index, precipitation, and temperature are reconstructed using the Fast Fourier Transformation (FFT) filtering algorithm.

## SUPPORTING INFORMATION

Additional Supporting Information may be found online in the supporting information tab for this article.

Text: Ratio of NBP (or $R_h$) amplitude to NPP amplitude: theoretical framework

Table S1-S6

Figs. S1-S15

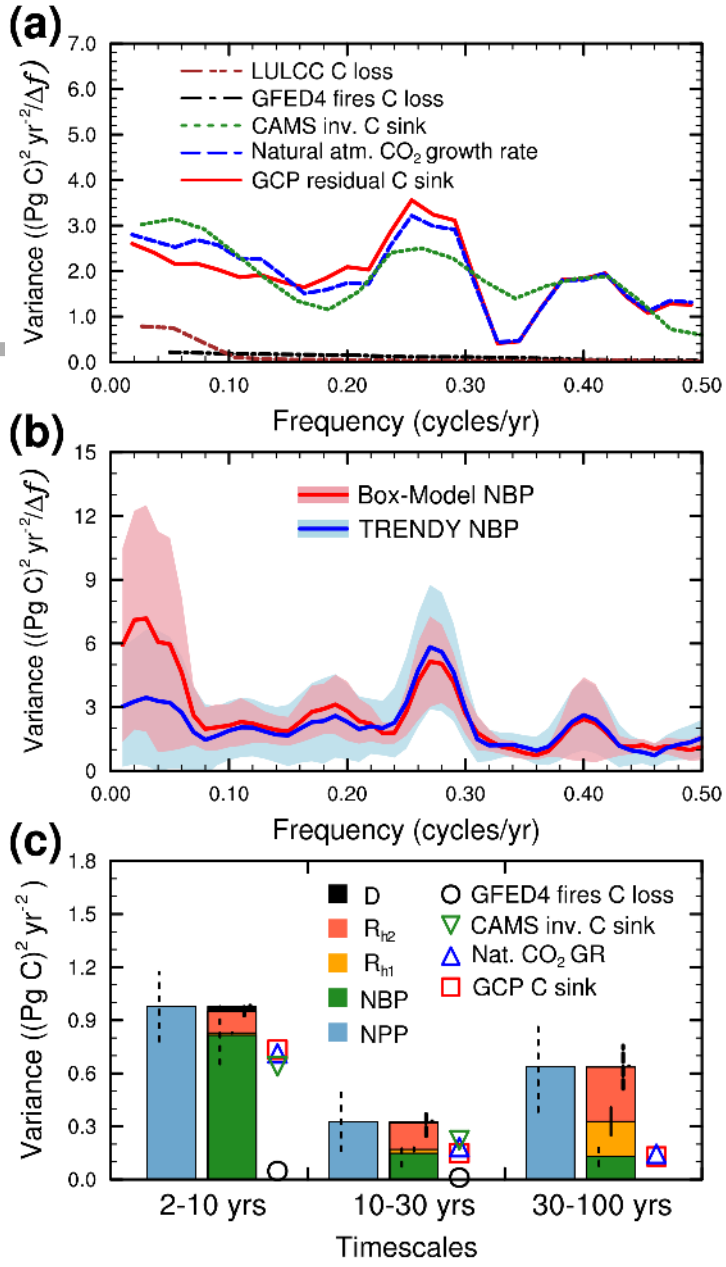


gcb_14275_f1.png

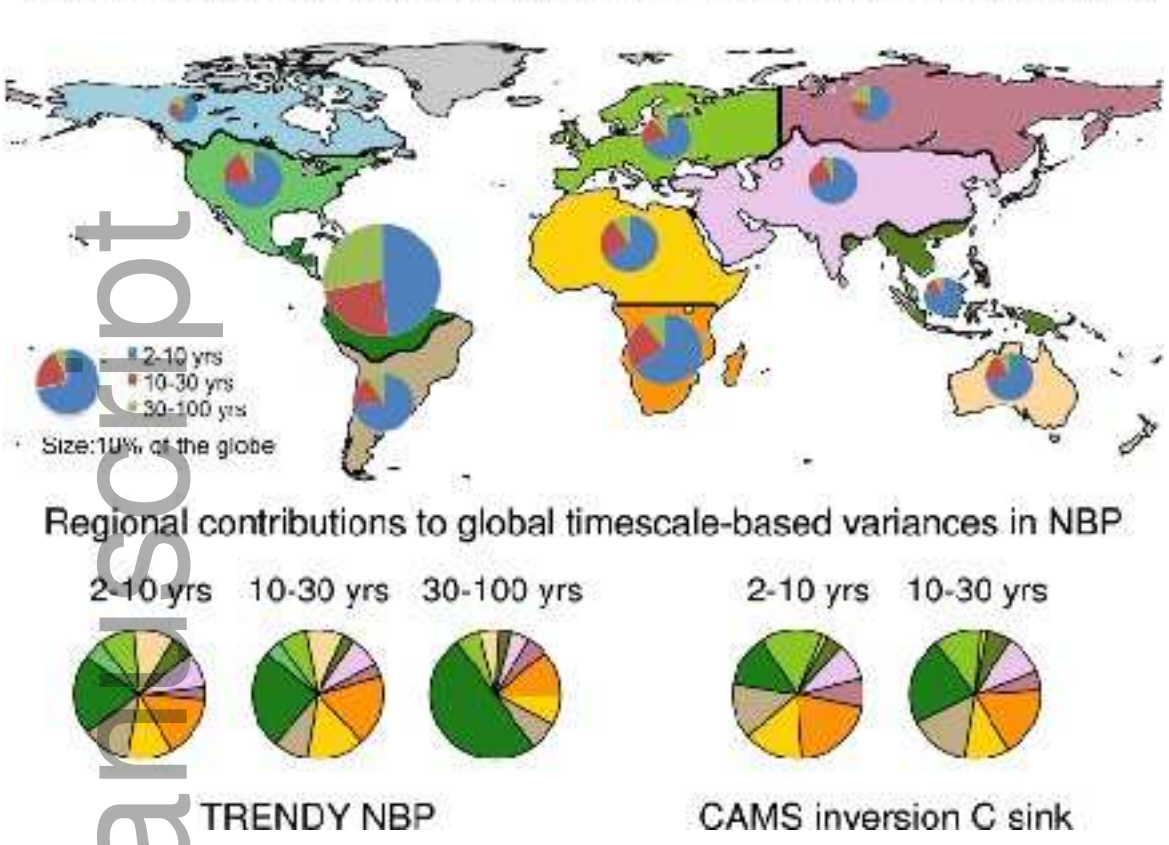


gcb_14275_f2.png

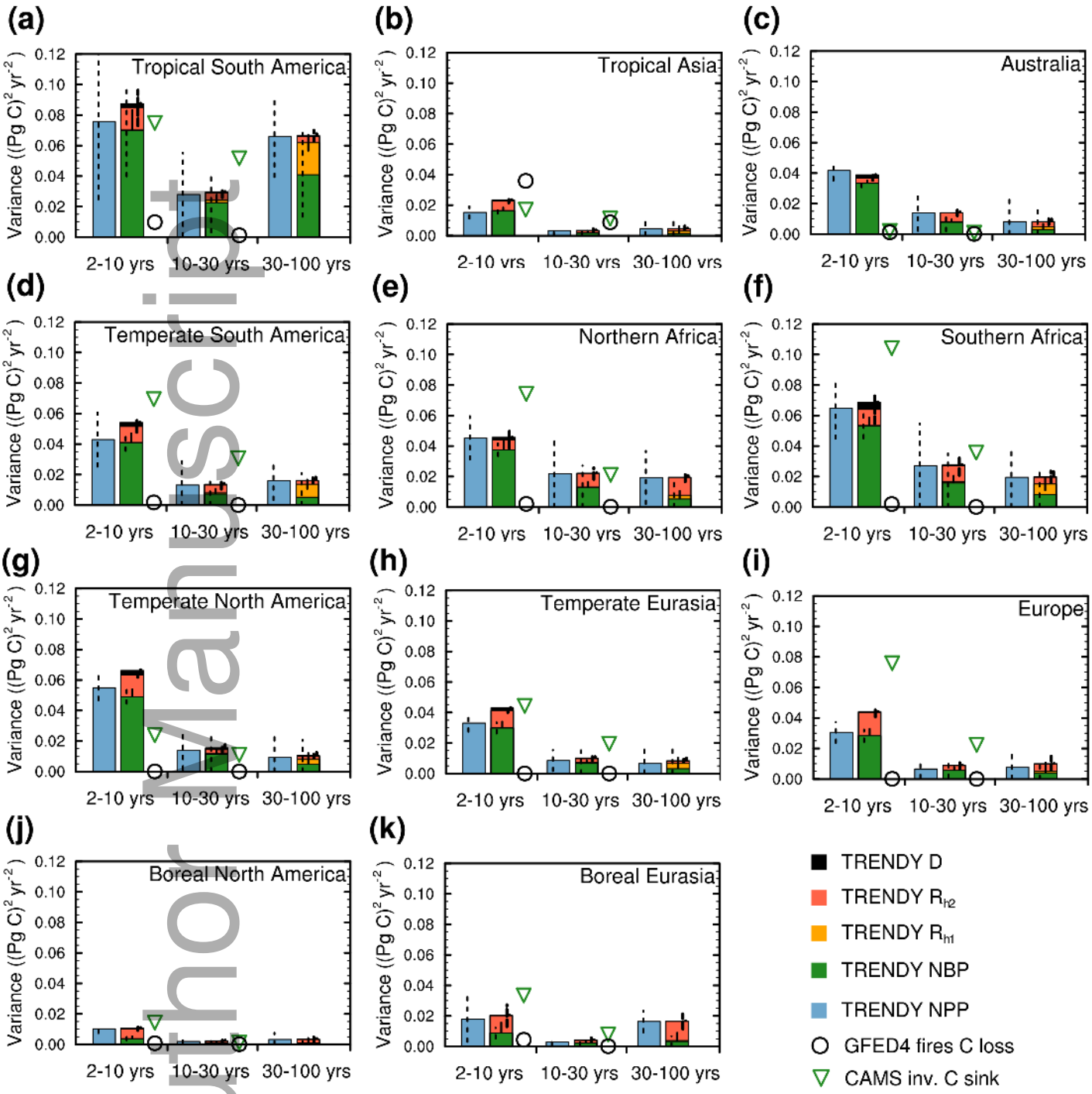


gcb_14275_f3.png

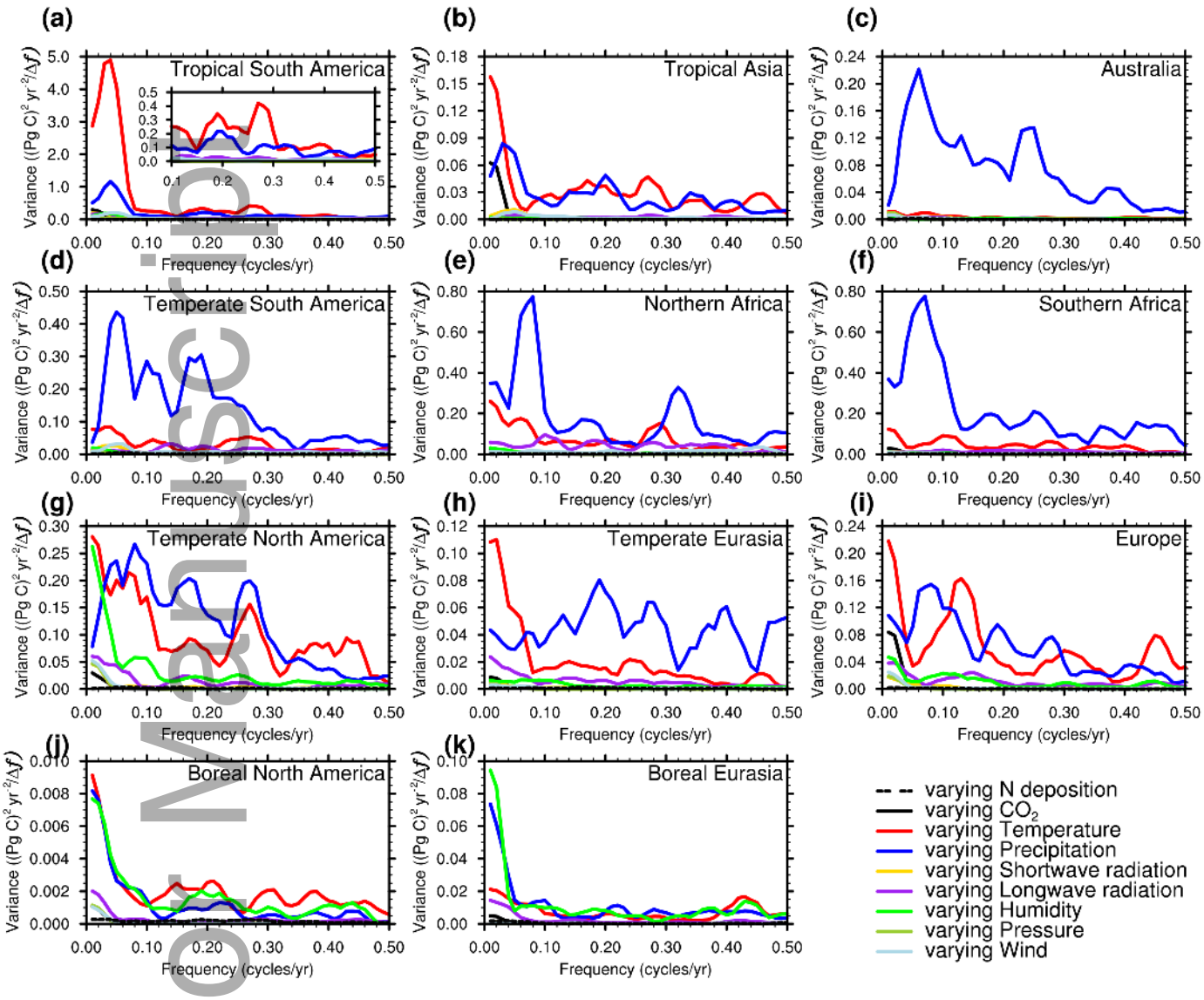


gcb_14275_f4.png

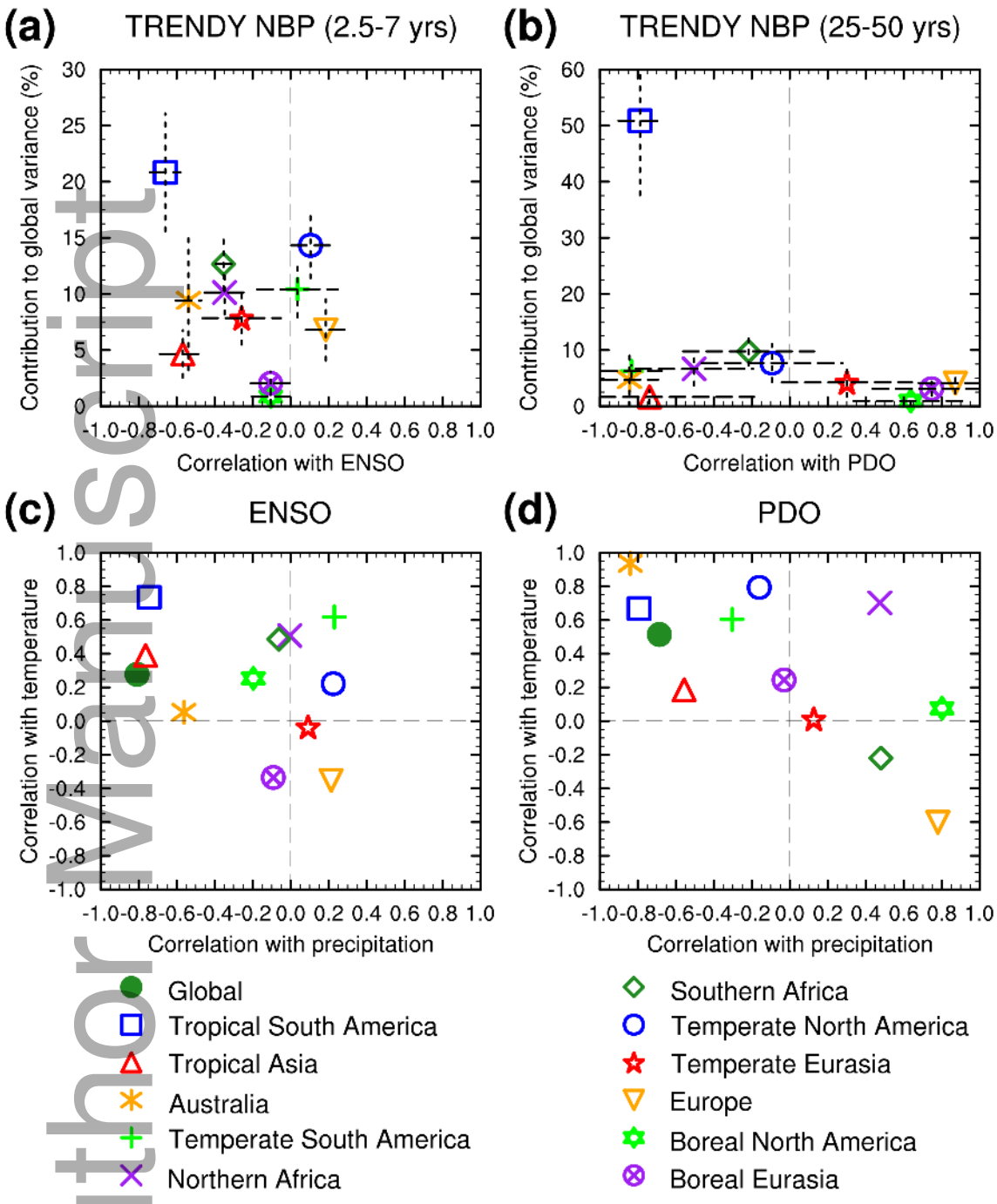


gcb_14275_f5.png